Caving 2026 – A van As, D Cumming-Potvin & J Wesseloo (eds)

doi:10.36487/ACG_repo/2645_01

Cave growth mechanism and surface subsidence in a structurally complex block cave: P0 case study

Erdenetogtokh Bayar [a,*], Johnson Ooi [a], Zoljargal Naranzorig [a], Delgerjargal Mendbayar [a], Munkh-Erdene Ulziijargal [a], Boldbayar Khurmyet [a], Ian Brunton [b]

[a] *Oyu Tolgoi, Rio Tinto, Mongolia*

[b] *ITASCA, Australia*

Abstract

This paper examines cave propagation and surface subsidence at the Panel 0 Block Cave, Oyu Tolgoi, developed within a deep (~1,300 m) and structurally complex rock mass. Cave growth was strongly controlled by major faults, persistent discontinuities, and low-strength fractured zones, evolving from stress-driven yielding at depth to structurally guided propagation upward, reaching the surface in ~36 months. Measurable subsidence began in Q1 2025, with its geometry and rates reflecting pronounced structural anisotropy. Integrated monitoring data and numerical modelling were used to reconstruct cave evolution and interpret the governing failure mechanisms.

Keywords: *cave propagation mechanism, plug subsidence, rock mass dilation, Panel 0*

1 Introduction

Oyu Tolgoi (OT) is one of the largest porphyry copper and gold deposits that consisting of a series of orebodies located in the southern Gobi region of Mongolia in Umnugobi province. The mine site lies approximately 550 km south of the capital city, Ulaanbaatar, and 80 km north of the Chinese border. The location of the mine can be seen on the map in Figure 1a, and Figure 1b depicts the orebodies which are being extracted at OT. Mining at OT commenced in early 2010 with open-pit operations. At the same time, underground infrastructure development began to enable mining of orebodies located approximately 1,300m below the surface. Ore extraction from underground began in 2022, with the first mining Panel 0 (P0), Hugo North Lift-1. Due to ore extraction, it altered the stress state of the surrounding rock mass leading to structural activation and eventually, violent seismic responses started appearing within the mining environment. With the completion of drawbell construction phase at P0, cave productivity was ramped up by increasing the material draw rate across P0 which allowed for better management of the cave health. The early stages of the cave growth were managed by adjusting the localised draw rate targets for individual draw bells. As the cave matured, uniform draw rates were adopted to ensure the cave was propagating at an even and balanced rate. The entire Hugo North orebody contained major structures which comprised weaker geological domains, as well as intensive minor and major structures within the cave column. Comparisons of observed cave propagation behaviour and surface subsidence development with published block caving and subsidence datasets highlighted both similarities in global caving propagation trends and distinct deviations which is attributable to the unique structural fabric of the OT deposit. The synthesis of modelling and monitoring results provides an improved mechanistic understanding of the structural controls governing cave propagation, breakthrough processes, and surface ground responses. This has direct implications for ongoing geotechnical risk management and future panel design strategies at OT mine.

* Corresponding author. Email address: erdenetogtokhb@ot.mn

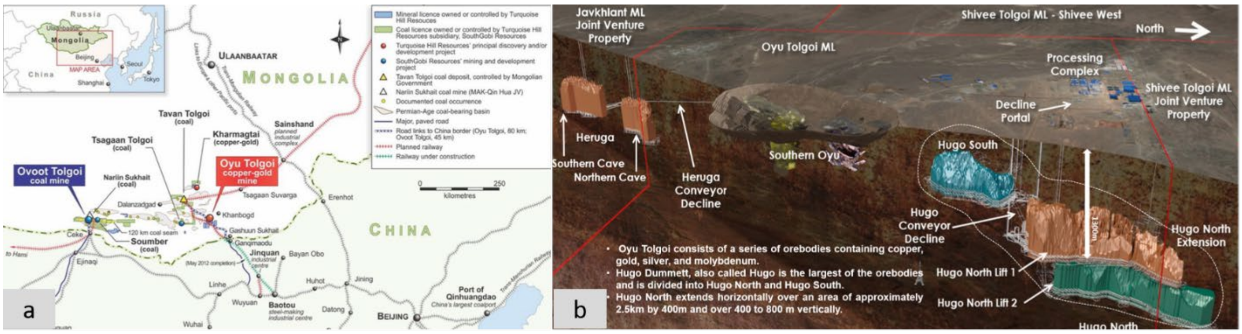

Figure 1 (a) Mine site location; (b) Series of open cut and underground orebodies

2 Geology and geotechnical condition at HNL1

The Hugo North deposit contains porphyry-style mineralisation and related alteration associated with quartz monzodiorite (QMD) intrusions, beneath a deformed sequence of upper Devonian and lower Carboniferous sedimentary and volcanic rocks. The deposit is an elongated body aligned to the north-northeast and extending for over 3 km. The Hugo North deposit hosts an easterly dipping sequence of volcanic strata and QMD intrusive rocks. The stratigraphically lowest rocks in the sequence consist of basalt flows and minor volcanic strata (Va), overlain by a dacite tuff and breccia (IGN) sequence.

Two groups of discontinuities are recorded at OT. These are:

- Major and intermediate structures: these represent regional, mine-scale, and block-scale faults
- Minor structures: these structures represent joints logged during face mapping or during drillcore logging.

The Hugo North deposit occurs within easterly-dipping homoclinic strata contained in a north-easterly elongate fault-bounded block. The northern end of this block is cut by several northeast-striking faults near the northern boundary.

2.1 Faults and major structures

The OT deposit is underlain by a complex network of faults, folds, and shear zones. Most of these structures are poorly exposed on the surface and have been defined through an integration of detailed exploration data primarily drillhole and underground mapping data, property-scale geological mapping, and geophysical data. Figure 2 depicts a series of large-scale structures across the entire footprint, both in the same orientation as the orebody and in various rock domains, which exhibit different behaviours under mining.

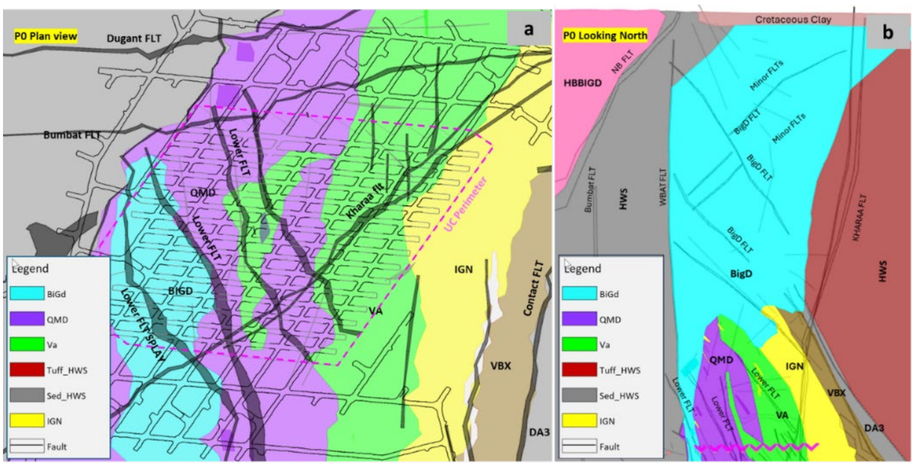

Figure 2 (a) Plan view and (b) section view Panel-0 Hugo North Lift 1 geological model indicate the major lithological features and structures

2.2 Rock mass properties at Oyu Tolgoi

The rock mass properties at OT are typical of massive to moderately veined porphyry deposits. Much of the rock is moderately to heavily microdefected, such that the core often breaks easily when it is handled. Examination of drillcore suggests that many of the features logged as planar open joints might be more appropriately counted as irregular closed (healed) microdefects that have opened during drilling. While stronger micro defects tend to remain healed and uncounted as fractures (although their density is noted qualitatively), neighbouring weaker micro defects that have opened are regularly counted as open joints. Extensive laboratory testing of diamond drillhole core samples was conducted during OT feasibility study in 2023 in order to update the intact rock strength properties for the various geotechnical domains at OT. Sample collection and testing targeted spatial distribution across Hugo North Lift 1 for of uniaxial compressive strength, triaxial compressive strength, and uniaxial tensile strength. It also targeted sufficient coverage to account for the typical porphyry deposit domains which vary by lithologies, alteration and weak vein density. A Hoek–Brown failure envelope regression has been performed on the test data, and the results are tabulated in Table 1.

Table 1 Oyu Tolgoi geotechnical characterisation: P0 dominant rock mass properties (SRK Consulting 2022)

Lithology code (P0)	Alteration	Geotechnical domains units	σ_{ci} (avg.) (MPa)	σ_{ci} (std.) (MPa)	σ_{ci} (P50) (MPa)	σ_{ci} (P30) (MPa)	m_i (avg.)	m_i (P50)
QMD	Advanced argillic alteration	BGU04	55.7	16.7	55.7	46.9	16.0	16.0
BiGd	UNALT (low vein density)	BGU01a	115.9	21.4	113.9	103.5	12.3	12.1
Va-IGN contact	–	BGU16b	76.8	29.3	71.7	59.1	12.0	11.0
Va (DA1b)	AAA	BGU17	66.2	13,24	64.9	58.5	17.1	16.8

3 Methodology

The methodology adopted in this study integrates cave numerical modelling with a comprehensive geotechnical monitoring program to evaluate the caveability and behaviour of the caving mechanism. A calibrated 3D numerical model was developed to simulate the cave propagation, stress redistribution, and associated deformation mechanisms under varying geological and operational conditions. The model incorporates site-specific geotechnical parameters and structural and orebody geometry to reproduce realistic cave growth and assess potential zones of stable section within the cave column. Complementing the modelling effort, an extensive monitoring framework comprising microseismic data, displacement measurements, and real-time in situ instrumentation was implemented to capture actual rock mass behaviour and assess caving performance. The integration of modelling outputs with observational monitoring data allows for continuous validation of model assumptions, refinement of predicted cave behaviour, and enhanced understanding of ground response throughout the caving stages.

3.1 Cave numerical assessment

The caving and stress redistribution processes inherently involve large deformations, shear along pre-existing joints and bedding surfaces, fracturing of intact rock blocks and fragmentation of the rock mass. Ideally, one would model this process using a pure discontinuum approach with explicit breakage of rock blocks. However, the computational cost and time requirements for solving mine-scale problems make it currently impossible to fully address the problem using the discontinuum approach (Sjöberg 2017). The caving process used for the analyses was implemented using the coupled cave propagation simulation method described in Hebert & Sharrock (2018). This method implements a detailed and accurate approach to simulate cave propagation based on strong bi-directional coupling between FLAC3D and CAVESIM.

3.2 Cave monitoring

Complementary monitoring systems confirmed rock mass conditions within the orebody and tracked cave propagation to surface, controlled by pre-existing structures and weaker lithological domains. Direct and indirect measurements – open holes, an Elexon cave tracker system, and geological features across P0 – consistently indicated upward cave growth, with surface breakthrough occurring a few months earlier than modelling prediction. Cave back monitoring equipment, including Elexon beacons, networked smart marker, and detector chains were installed 2 years before undercutting is commenced through slimline deep boreholes with length of 1,200 m from the surface. Cave deformation and material flow were indirectly tracked, while multiple open holes provided direct evidence of changes in ground conditions over time. Table 2 summarises the monitoring techniques at OT P0, with Figure 3 illustrating the comprehensive system in 3D view.

Table 2 Summarises the type of monitoring techniques applied to the P0 cave and surface subsidence measurement

Target	Technique	Type	Objective
Subsurface monitoring	Indirect	Microseismic	Record cave back seismicity and potential damage zone close the underground tunnels
	Indirect	Geo4Sight NSM	Radio signal communication between the sensors to monitor rock mass fracturing, referencing the initial installation position
	Indirect	Elexon cave trackers	Magnetic field tracking within the orebody to understand the flow mechanism of the material overlying the production level
	Direct	Open hole observation using borehole camera	Repeated camera surveys of open holes to identify the changes in borehole stability and sidewall damage progression
Surface change monitoring	Direct	Prisms and total stations	Surveying of prisms the surface to measure the depression rate
	Indirect	Interferometric synthetic aperture radar (InSAR)	Satellite measurement of surface displacement
	Indirect	Lidar drone surveys	Digital survey records used to detect surface displacement between different time periods.

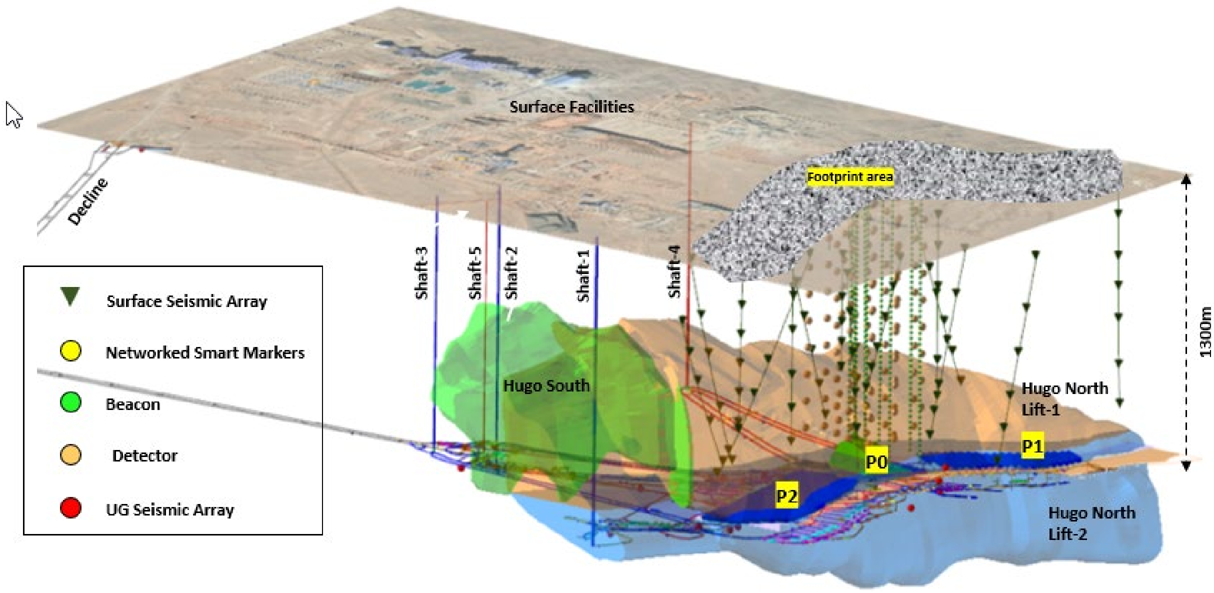

Figure 3 Cave monitoring systems installed around the footprint area and Panel 0 cave for Hugo North Lift-1

3.2.1 Subsurface instrumentation

3.2.1.1 Seismic monitoring

OT mine has invested in a larger seismic sensor array comprising 138 predominantly triaxial sensors with over 400 active data channels. The purpose of the microseismic system is to provide information for cave growth monitoring and to evaluate seismic risk around the mine. The cave area is largely covered by an array of 90 triaxial sensors installed and grouted in 15 boreholes which were drilled from surface. The boreholes deep surround the orebody, as shown by the green triangles in Figure3.

3.2.1.2 Network smart markers, beacon, and cave tracker system

Network smart markers (NSM) and tilt markers were installed to monitor caving during the mining of P0. Both are serving similar monitoring purposes and transmit data via radio signals. Tilt markers can measure magnitude of the deformation with the dipping angle changes in degrees while the networked smart markers giving the idea of how the rock mass start fracturing over the time via radio signal strength index changes. Tilt amplification reflects progressive rock mass damage and yielding in the vicinity of the borehole, associated with fracture development in response to caving activity. Data observations indicated that tilt markers become more active, exhibiting incremental changes in the radio signal strength indicator (RSSI), as the deformation zone expands and approaches geological structures. This behaviour predominantly reflects the separation of larger rock blocks along structural features and the progressive yielding of the rock mass induced by material drawn from the underground excavation horizon (Kamp et al. 2024).

3.2.1.3 Surveying of the open holes

Surveying of open holes was found to be a critical in determining the position for direct measurement of the cave back as mining caving progressed. Figure 4 displays common borehole failure types observed down the open holes drilled for P0 where faults were intersected. A section of the borehole damage that has been observed throughout the inspection periods, which generally coincides with fault intersection. Footage was collected using a motorised camera unit that runs down the borehole to capture the condition of the rock mass and assess behavioural changes in response to caving. Figure 5 illustrates the progression of damage along the borehole between 700 and 900mRL. The camera, struggled to pass beyond the deforming borehole which was experiencing squeezing in the early days of the cave when production was still ramping up. A clear correlation was observed between elevations showing excessive borehole damage and changes in RSSI amplitude from networked smart markers.

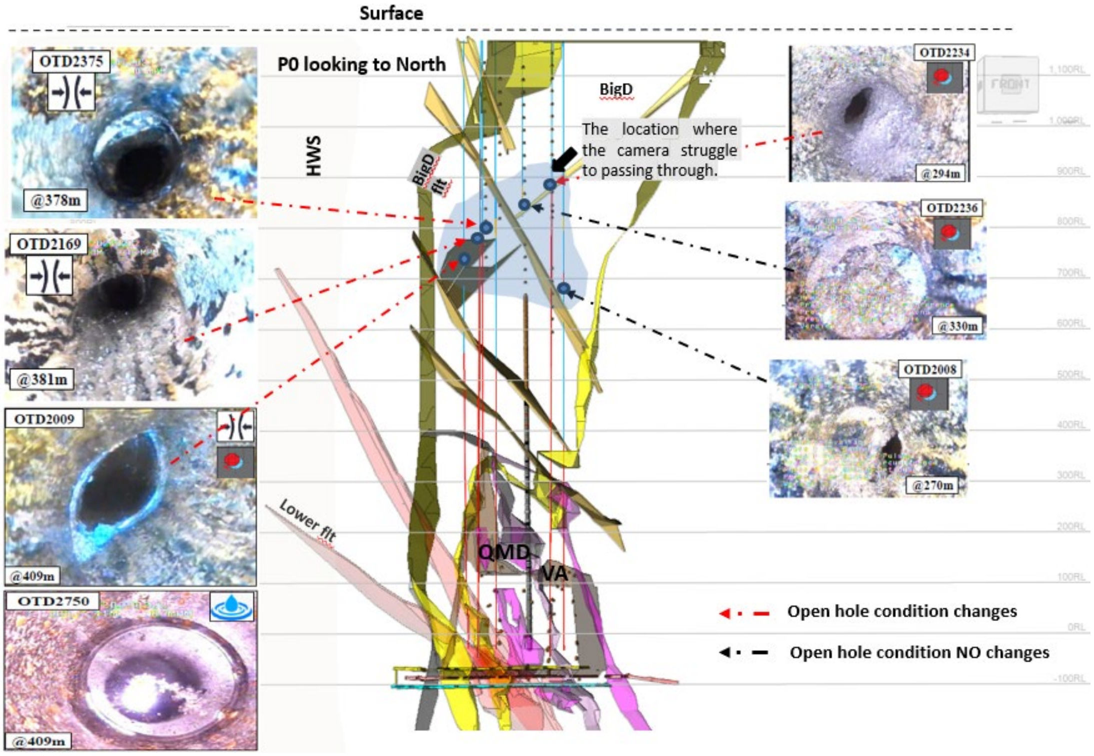

Figure 4 **Common borehole failure type at P0 open holes (borehole shifting, squeezing presences)**

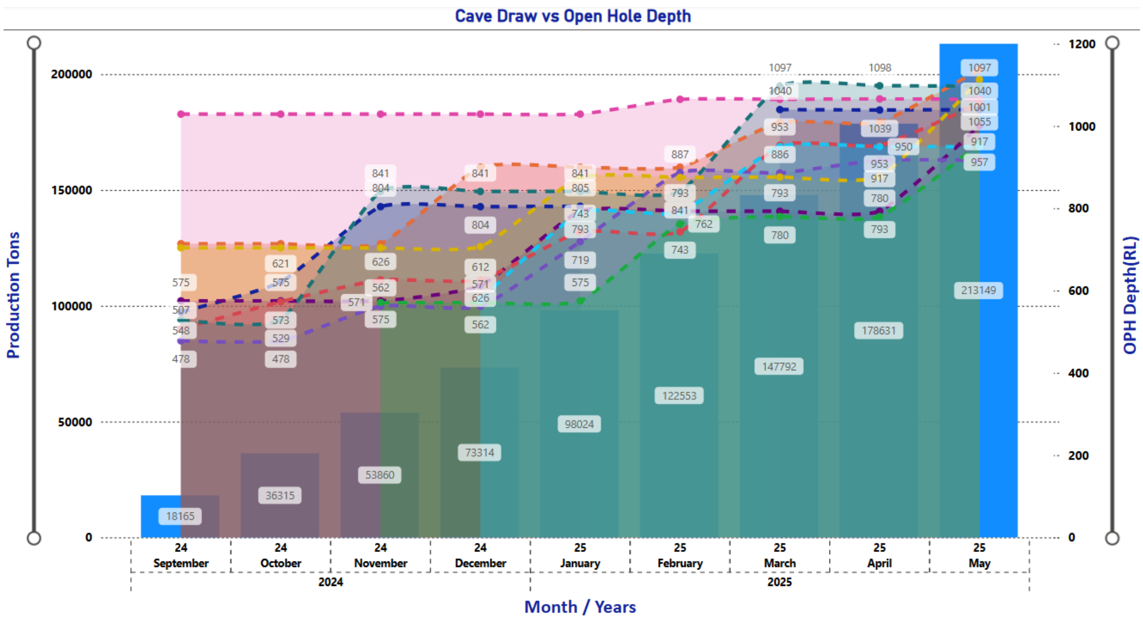

Figure 5 **P0 open holes damage progression over time compared to the material draw from the extraction level**

3.2.2 Surface depression monitoring

As cave propagation advanced to the surface within the cave zone, it became critical to understand how the subsurface changes could influence surface topography, including depressions and lateral deformation. The monitoring techniques are also helpful to define exclusion zones where development or personnel access is restricted. These zones typically include any area above the mining footprint and extend a given distance beyond the predicted life-of-mine crater and fractured zone. This also helps to mitigate risks to personnel, equipment, and infrastructure.

3.2.2.1 Prism monitoring and surface elevation changes

The surface cracks around the periphery of the cave and the crack extent follows the structure orientation, and the level of deformation increased within the perimeter of the caving zone. Initial planning deformation levels predicted for the mining of the P0 footprint. The prism monitoring involving the robotic total station TS-60 has been used for the surveying of the prisms permanently installed on the stable ground of the surface are included in the cave numerical assessment and deformation levels at the surface.

3.2.2.2 Interferometric synthetic aperture radar

The objective of InSAR imaging is to detect, measure, and monitor surface topographic changes in elevation and their movement patterns through regular data collection every 11 days. InSAR is part of a complementary system that validates observations for entire mine infrastructures across wider areas.

4 Cave propagation and surface subsidence

4.1 Cave seismic responses at different stages

Cave behaviour changed over time during the mining of P0, following the stages of undercutting, drawbell development, and production ramp-up. Figure 6 shows how the seismic response evolved during these different stages. The first 12 months of undercutting, seismic activity increased as the cave void was created by blasting. By 2023, stable production had started, and the seismic response became closely related to the material draw rate. Seismic activity continued to increase steadily until the second half of 2024. Later in 2024, there was a significant decrease in seismic activity likely linked to the cave back propagated higher in the cave column, where intensive geological structures are presented. These structures may have reduced the overall rock mass response. Over time, pre-existing geological structures began to control the spatial development of the cave. The acceleration of the cave deformation front was primarily driven by a rapid loss of rock mass confinement, resulting in the detachment of material from the cave back. At the same time, a reduction in the seismic activity was observed, suggesting a shift in cave propagation mechanisms from a stress-driven regime to structural controlled cave responses.

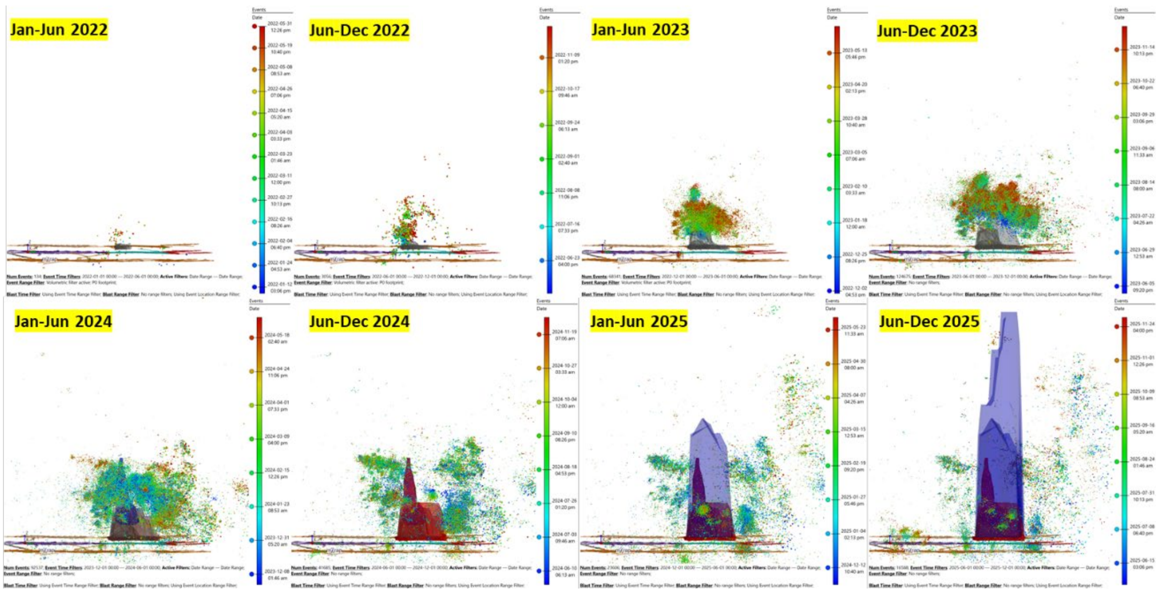

Figure 6 P0 seismic evolution in section view since commencement of undercutting

4.2 Cave tracker and Geo4Sight Interpretation

In September 2024, a noticeable increase in offline detectors were observed, primarily due to exhausted rock mass conditions around the cave production zone. As a result, the offline status of these detectors progressively migrated to higher elevations along the orebody column in the subsequent months. This upward shift led to the development of blind zones in the tracking of beacons embedded within the orebody, thereby making the estimation of the cave back extremely challenging. This situation necessitated using the NSM as the primary tool for estimating the cave-yielded zone, rather than continuing to rely on the first drop of the beacons spaced at 25 m intervals in a daisy-chain configuration, which had previously been used to determine the cave back. The networked smart markers played a crucial role in delineating the yield zone boundary, whereas beacons serve a distinct purpose in monitoring the cave back and material flow of the failed rock mass within the caving zone. NSM marker tilt used of caving changes compared with seismic activity in the proximity of the markers are part of the verification tools in the early caving stages to understand damage progression within the rock mass. Figure 7 shows the correlation between tilt data from the selected marker and seismic events within a 25 m radius along the smart marker borehole. Amplification of the NSM tilt over time followed by a decrease in seismic events around the borehole section suggested that the rock mass yielding process followed the decreasing seismic activity trend. The tilt data has enriched the cave information and is used to confirm the rock condition above the cave (Bayar et al. 2024).

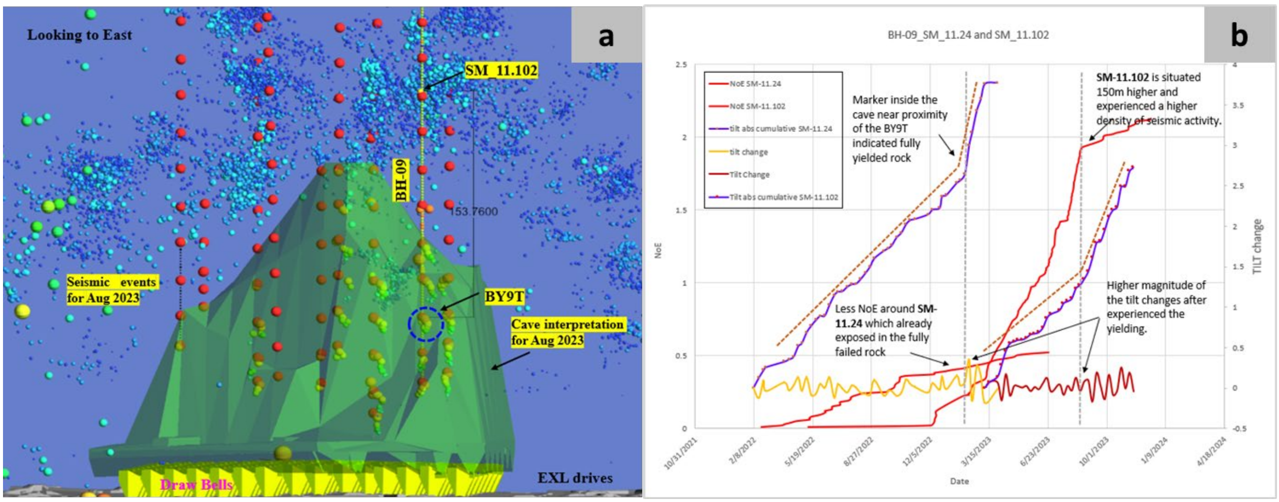

Figure 7 (a) Cave frame interpretation August 2023 using the beacon and network smart markers; (b) Absolute tilt changes over time compared with seismicity

Figure 8 illustrates the cave yield zone development based on the active NSM channels for each quarter since NSM started to be utilised as the primary data for cave yield zone frame interpretation in the second quarter of 2025. Tracking of, regardless of rock mass variability and domain differences, has shifted to rely on the location of the deepest active marker in each of the instrumentation chains. The section views below in Figure 8 shows 3 of the instrumentation boreholes as an example of the cave deformation front tracking and its elevation migration, generally following the presence of structures within the caving zone overlying the cave back.

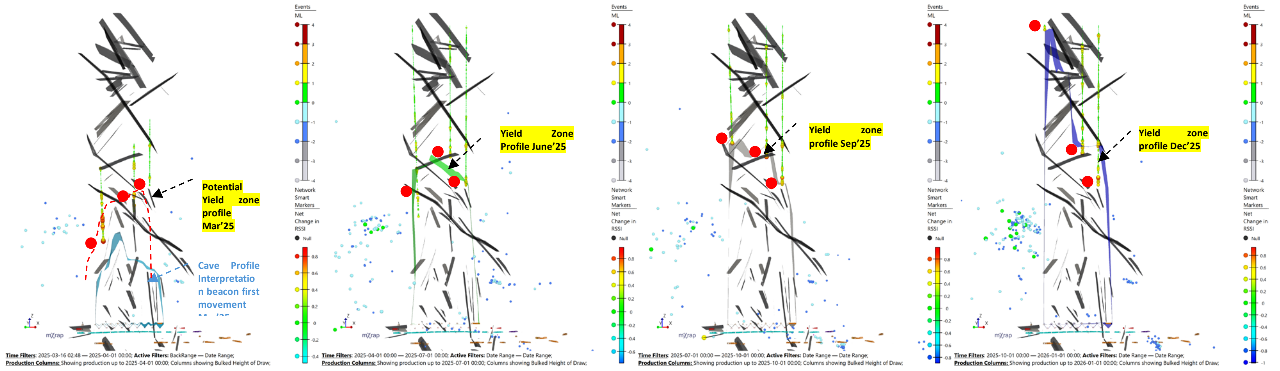

Figure 8 Panel 0 beacon network smart marker holes (radio signal strength indicator amplification in the faulted region, where the indication of rock mass separation along the pre-existing joint and structure plane), section view looking to the northeast. Cave frame interpretation for the end of each period

4.3 Cave modelling and mechanism

Caveability modelling has evolved over the past 5 years as site monitoring and cave interpretation data have become available. The key findings from this process include that early modelled cave propagation was characterised by rapid caving and chimneying in the southwest corner of the footprint, shown in Figure 9. To emulate the observed behaviour, the following model properties were considered important: fault spatial distribution and associated shear strength properties. Modelled propagation is strongly controlled by faults, particularly large continuous structures and lower rock mass strength lithological contact zones. The BIGd-QMD contact zone was of importance for the development of the early chimney in the southwest region of the footprint. Initial model assumptions for this were in the range of 1.15 to 1.20, based on industry benchmarks. As additional monitoring data became available, an improved model calibration fit to interpreted cave geometry was made by assuming bulking factors in the order of 1.08 to 1.10.

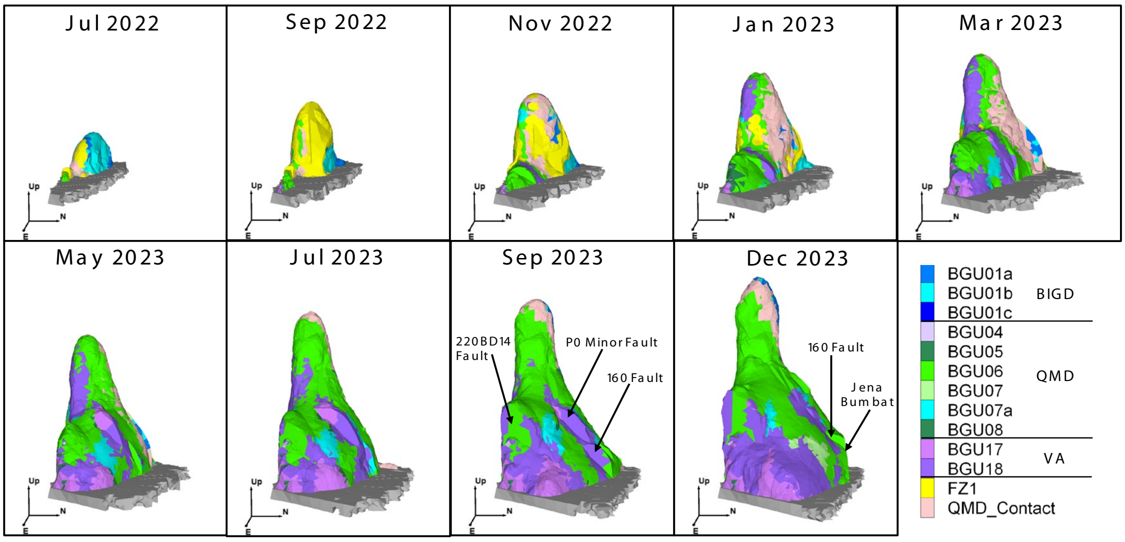

Figure 9 Calibrated modelled cave geometry with respect to observed early chimney development (July 2022 to December 2023)

Cave monitoring methods and interpretations of cave geometry from available data vary between operations. Figure 10 illustrates the conceptual caving model, compared with the observed rock failure mechanism on the right-hand side, as defined by the site interpretation. Due to the different nature of the orebody and host rocks, many factors can influence cave progression and the resulting interpretation of the cave profile, including geological and geotechnical properties and the geometry of lithologies, faults, and alteration (Kamp et al. 2024). OT P0 displays combination of stress-driven and structurally controlled cave propagation, where the early stages of the caving were more relevant to the typical (Duplancic & Brady 1999) conceptual model, as illustrated in Figure 10 below. The main driver of the cave propagation was the redistribution of stress changes, followed by rapid chimney development at the southwest of P0 in low-strength rock associated with fault zones. The presence of numerous minor and large-scale faults and vein networks within the cave column further promoted rock mass fracturing along pre-existing steeply dipping to subvertical structural planes. This structural control accelerated cave-front advance, as illustrated in Figure 10, where cave back progression was strongly influenced by weaker lithological domains. Subsurface cave monitoring data consistently indicated that P0 caving is predominantly structurally controlled. In addition to these factors, production draw control played a critical role in shaping the cave profile and directly influence the rate of cave maturity.

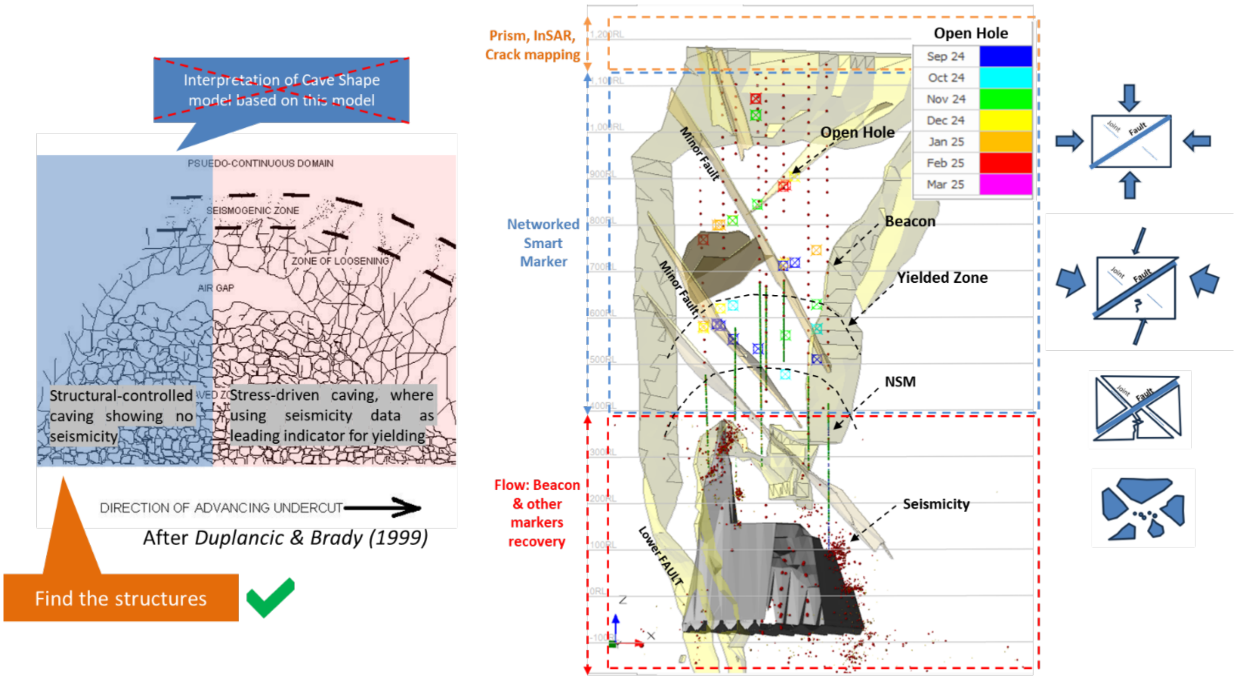

Figure 10 Duplancic & Brady (1999) caving mechanism model versus observed mechanism

Activation of faults in advance of the cave crown led to preferential cave development and early interaction with the surface. To match modelled surface displacements and fault shear behaviour, a global cave bulking factor of 1.08 had to be assumed. Figure 11 demarcated the results of the FLAC 3D cave propagation, cave surface interaction simulation using the lower bulking factors to fit the actual monitoring data.

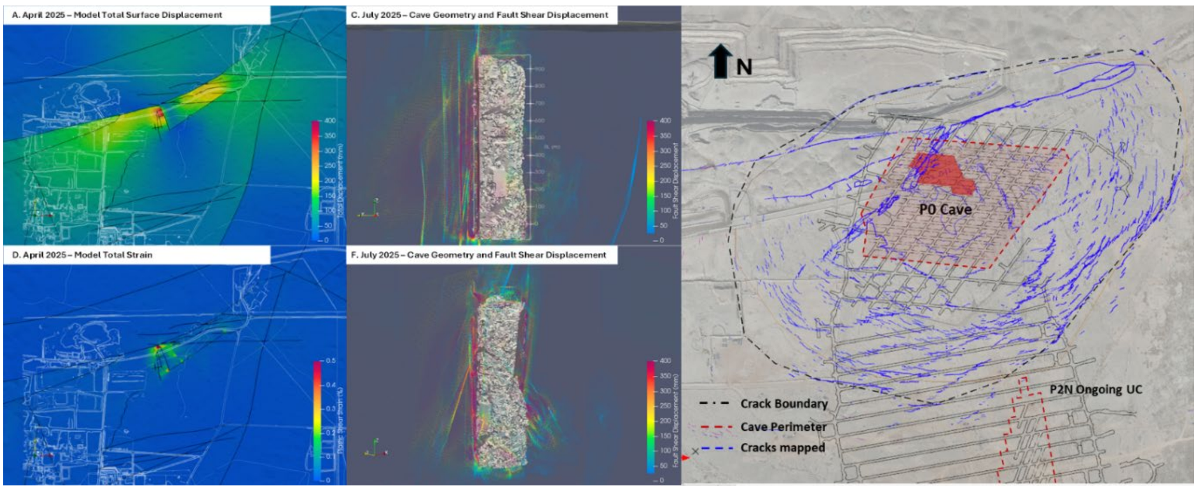

Figure 11 Modelled cave geometry and surface interaction (April and July 2025) and surface crack forming around the periphery of the cave (August 2025)

4.4 Surface subsidence and breakthrough

The surface subsidence assessment must account for environmental impacts, particularly surface cracking and deformation. Ground movements can disrupt surface water flow, necessitating hydrological analysis. Assessment is also important for the potential for surface infrastructure damage, which is necessary to protect mine infrastructure over the life of the mine. Surface subsidence and breakthrough terminology vary for the mines depending on the breakthrough process and rock mass damage. OT breakthrough mechanism is considered a plug subsidence with little potential for ratholing or a glory hole at a specific location. Since ratholing breakthroughs will not be observed in this specific environment, the criteria to confirm breakthrough events are as follows.

- Three NSM holes at the northern boundary were fully consumed by the cave in September 2025, with similar conditions subsequently observed in additional holes over the following months.
- >3 m surface depression was recorded both in InSAR or LiDAR measurement within the perimeter of the cave.
- Increasing damage or displacement acceleration were observed at the production level following the increase of vertical loading due to a breakthrough and structurally controlled plug subsidence event.

The breakthrough occurred via chimney piping bound by three major structures, to the west, the WestBat structure, the north, the Bumbat and to the East, the Kharaa fault structures. These structures become the external bounds for the chimney with deformation not occurring beyond them. Figure 12b presents the complete cave propagation mechanism P0 beginning with stress-driven processes during cave establishment, transitioning to structurally driven propagation within the cave column along weaker lithological boundaries, and finally triggering large-block mobilisation, manifested as plug cave subsidence and the conceptual definition of subsidence zones (Figure 12a) as per surface subsidence zone definitions (van As et al. 2003).

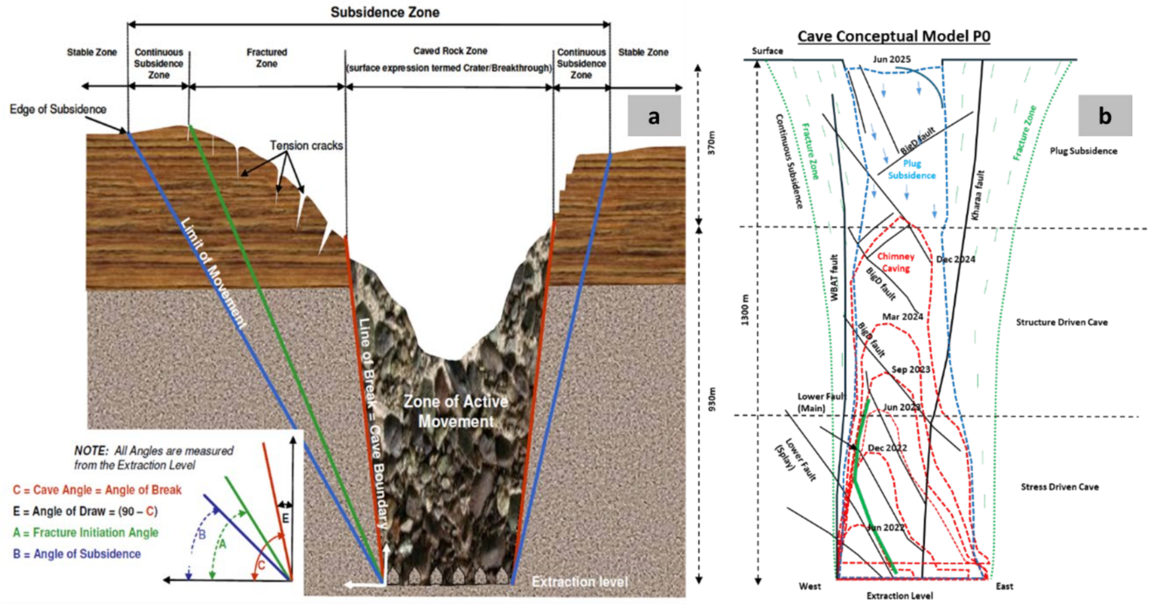

(a) (b)

Figure 12 (a) Surface subsidence zones definition; (b) Cave conceptual model for Oyu Tolgoi P0 Hugo North Lift-1 (van As et al. 2003)

4.5 Subsidence model performance

Model performance was compared to the data observed until July 2025, including InSAR displacement data, prism vector displacement. It should be noted that prisms were commissioned in May 2025, and InSAR data indicates that significant displacements in the assessment of 100 mm had have occurred by this time. A summary of the model comparisons with measured surface displacement is shown in Figure 13 for April 2025.

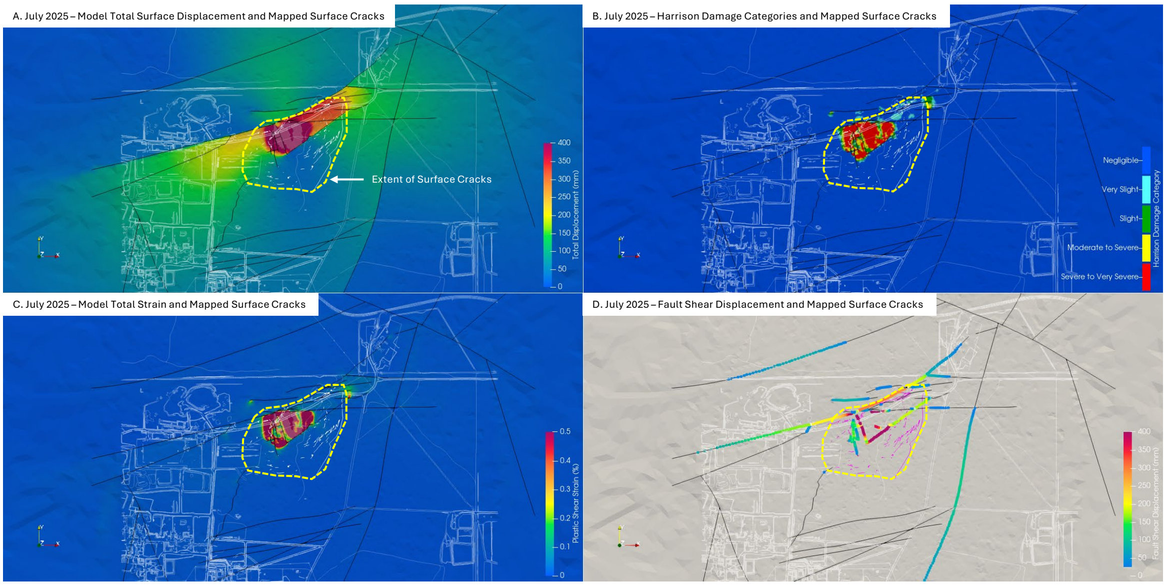

Figure 13 Modelled total surface displacement, total strain and fault shear displacement versus measured surface cracks in July 2025 (Harrison 2011 damage class)

P0 surface subsidence modelling shows displacements largely constrained between the north Boundary and Kharaa Faults, with zones of higher displacement aligned sub-parallel to the major principal stress. InSAR displacements are generally higher than model predictions and extend beyond both faults. Prism displacement orientations align well with the model, confirming the cave breakthrough area, and the timing of cave crown interaction with surface displacement consistent between measured data and the model. Figure 13 compares modelled surface displacement (Harrison 2011), strain, and fault shear displacement with surface cracking mapped in July 2025, indicating that observed cracking extends further south than predicted. Modelling highlights the importance of near-surface fault location and shear strength, consistent with field observations of significant fault shearing near the cave breakthrough zone.

5 Conclusion

Resource depletion at shallow depths is driving mining into deeper, more complex environments, where controlling mining-induced changes is challenging. This study presents the first breakthrough event in Panel 0, supported by years of data, monitoring, and simulation. While modelling predicted a breakthrough around July–August 2025, early cracks appeared in late 2024, confirmed by field observations, InSAR data, and multiple monitoring systems through 2025. These results showed cave propagation following major structures, forming a chimney-type cave propagation followed by the plug subsidence breakthrough mechanism confined by structural boundaries to the north NB fault, west WestBat fault and the east Kharaa fault. Overall, the cave draw strategy has supported controlled propagation and preparation for surface breakthrough.

Acknowledgement

We extend our sincere gratitude to everyone who contributed to the successful completion of this paper. We express our deepest appreciation to the members of our organisation for their invaluable guidance, expertise, and mentorship throughout the research process. We are also grateful to Oyu Tolgoi LLC for providing the necessary support and resources that made this work possible.

6 References

Bayar, E, Karta, S, 2023, 'Introduction to Oyu Tolgoi Advance monitoring systems design – integrated ground hazard and cave performance monitoring Systems', *IMS 33rd Annual Meeting* South Africa, Cape Town.

Bayar, E, Simanjuntak, K, Birch, D, Mardiansyah, F & Purwanto, H 2024, 'Seismological data and analysis for the early stages of block caving', in D Johansson & H Schunnesson (eds), MassMin 2024: *Proceedings of the International Conference & Exhibition on Mass Mining*, Luleå University of Technology, Luleå, pp. 893–908, https://doi.org/10.36487/ACG_repo/2435_G-02

Brown, ET 2002, *Block Caving Geomechanics: Issue 3 of JKMRC Monograph Series in Mining and Mineral Processing*, Julius Kruttschnitt Mineral Research Centre, The University of Queensland, St Lucia.

Caveros, P, Gaite, S, Lorig, LG & Gomez, P 2003, 'Three-dimensional analysis of fracturing limits induced by large scale underground mining at El Teniente mine' *12th Panamerican Conference on Soil Mechanics and Geotechnical Engineering*, American Rock Mechanics Association, Alexandria, https://www.researchgate.net/publication/259741745

Contreras, C, Elmo, D, Jakubec, J & Thomas, A 2022, 'Reviewing Laubscher's empirical method to estimate subsidence limits', in Y Potvin (ed.), *Caving 2022: Proceedings of the Fifth International Conference on Block and Sublevel Caving*, Australian Centre for Geomechanics, Perth, pp. 805–818, https://doi.org/10.36487/ACG_repo/2205_55

Cumming-Potvin, D, Wesseloo, J, Jacobsz, SW & Kearsley, E 2018, 'A re-evaluation of the conceptual model of caving mechanics', in Y Potvin & J Jakubec (eds), *Caving 2018: Proceedings of the Fourth International Symposium on Block and Sublevel Caving*, Australian Centre for Geomechanics, Perth, pp. 179–190, https://doi.org/10.36487/ACG_rep/1815_11_Cumming-Potvin

Harrison, P 2011, 'Mine subsidence', in P Darling (ed.), *Society of Mining Engineers Handbook*, Society for Mining, Metallurgy & Exploration, Englewood, pp. 627–644.

Hebert, Y & Sharrock, G 2018, 'Three-dimensional simulation of cave initiation, propagation and surface subsidence using a coupled finite difference–cellular automata solution', in Y Potvin & J Jakubec (eds), *Caving 2018: Proceedings of the Fourth International Symposium on Block and Sublevel Caving*, Australian Centre for Geomechanics, Perth, pp. 151–166, https://doi.org/10.36487/ACG_rep/1815_09_Hebert

Kamp, C, Cumming-Potvin, D, Lett, J, Poulter, M, Shea, N, Jalink, B & Vanegas-Palacio, C 2024, 'Cave profile interpretation using instrumentation and the cave conceptual model', in D Johansson & H Schunnesson (eds), *MassMin 2024: Proceedings of the International Conference & Exhibition on Mass Mining*, Luleå University of Technology, Luleå, pp. 318–349, https://doi.org/10.36487/ACG_repo/2435_C-02

Lett, J 2024, 'Geotechnical lessons learnt during undercutting in deep caving at Cadia Operations', in P Andrieux & D Cumming-Potvin (eds), *Deep Mining 2024: Proceedings of the 10th International Conference on Deep and High Stress Mining*, Australian Centre for Geomechanics, Perth, pp. 109–136, https://doi.org/10.36487/ACG_repo/2465_02

Sjöberg, J, Perman, F, Lope Álvarez, D, Stöckel, B-M, Mäkitaavola, K, Storvall, E & Lavoie, T 2017, 'Deep sublevel cave mining and surface influence', in J Wesseloo (ed.), *Deep Mining 2017: Proceedings of the Eighth International Conference on Deep and High Stress Mining*, Australian Centre for Geomechanics, Perth, pp. 357–372, https://doi.org/10.36487/ACG_rep/1704_25_Sjoberg

SRK Consulting, 2022, *OT Geotechnical Characterisation – P0 Dominant Rock Mass Properties, R_01-1092-02_SRK_RTINTO*, Vancouver.

Van As, A, Davison, J & Moss, I 2003, *Subsidence Definitions for Block Caving Mines*, Rio Tinto technical report.